Chromatically Corrected Multicolor Multiphoton Microscopy

Hugo Blanc, Gabriel Kaddour, Nicolas B David, Willy Supatto, Jean Livet, Emmanuel Beaurepaire, Pierre Mahou

ACS Photonics

pubs.acs.org/journal/apchd5
Letter

Chromatically Corrected Multicolor Multiphoton Microscopy

Hugo Blanc, Gabriel Kaddour, Nicolas B. David, Willy Supatto, Jean Livet, Emmanuel Beaurepaire,* and Pierre Mahou*

Cite This: https://doi.org/10.1021/acsphotonics.3c01104
Read Online

ABSTRACT: Simultaneous imaging of multiple labels in tissues is key to studying complex biological processes. Although strategies for color multiphoton excitation have been established, chromatic aberration remains a major problem when multiple excitation wavelengths are used in a scanning microscope. Chromatic aberration introduces a spatial shift between the foci of beams of different wavelengths that varies across the field of view, severely degrading the performance of color imaging. In this work, we propose an adaptive correction strategy that solves this problem in two-beam microscopy techniques. Axial chromatic aberration is corrected by a refractive phase mask that introduces pure defocus into one beam, while lateral chromatic aberration is corrected by a piezoelectric mirror that dynamically compensates for lateral shifts during scanning. We show that this light-efficient approach allows seamless chromatic correction over the entire field of view of different multiphoton objectives without compromising spatial and temporal resolution and that the effective area for beam-mixing processes can be increased by more than 1 order of magnitude. We illustrate this approach with simultaneous three-color, two-photon imaging of developing zebrafish embryos and fixed Brainbow mouse brain slices over large areas. These results establish a robust and efficient method for chromatically corrected multiphoton imaging.

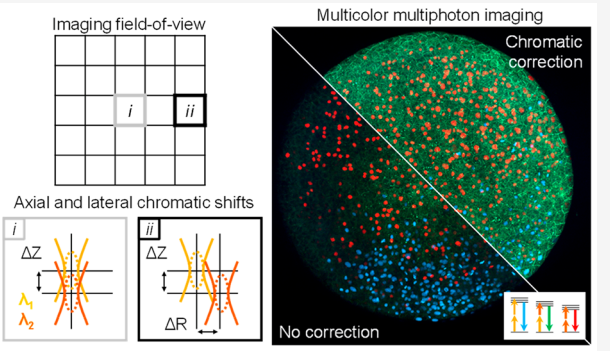

KEYWORDS: *chromatic aberration, adaptive optics, multicolor fluorescence imaging, two-photon microscopy, mouse brain, zebrafish embryo*

INTRODUCTION

Imaging multiple cellular and molecular agents in their natural environment, i.e., in tissues, is essential for analyzing complex biological processes. To this end, a wide range of labels, sensors, and reporters based on spectrally distinct fluorescent proteins have become available.[1,2] Multiphoton fluorescence microscopy[3,4] is now routinely used to image these markers in fields ranging from neuroscience[5,6] to immunology[7] and developmental biology[8] thanks to its ability to visualize cell morphology and dynamics in situ. The last two decades have seen considerable technological advances in imaging speed and depth as well as field-of-view area,[9] spatial adaptive optics to preserve resolution in complex environments,[10] and spectral unmixing.[11,12]

Strategies for simultaneous multiphoton excitation of multiple chromophores have been actively explored using either broadband laser pulses[13−15] or multiple narrow-band pulses.[16,17] However, chromatic aberration remains an important bottleneck in the development of color multiphoton imaging with multiple excitation wavelengths. In particular, in point-scanning microscopy, chromatic aberration can be decomposed in two terms: axial and lateral chromatic aberrations. These two terms are both introduced by the optics present in the scanning path and cause two focused beams centered at wavelengths λ_1 and λ_2 to be shifted axially and laterally during the scanning of the beams (Figure 1).[18] Therefore, the ability to perform multicolor imaging without compromising spatial and temporal resolution, field-of-view size, and signal-to-noise ratio is hampered. Lately this problem became even worse with the development of three-photon microscopy, expanding the range of excitation wavelengths from 700 to 1700 nm.

In this context, chromatic aberration between two focused beams centered at wavelengths λ_1 and λ_2 was initially corrected by using a pair of lenses to adjust the axial foci of the beams relative to the imaging plane of the microscope objective.[19] However, this introduces an amount of spherical aberration that increases with defocus, resulting in degraded axial resolution.[20] Pure defocusing applied to one of the two beams using phase modulators was later proposed, for example

Received: August 2, 2023

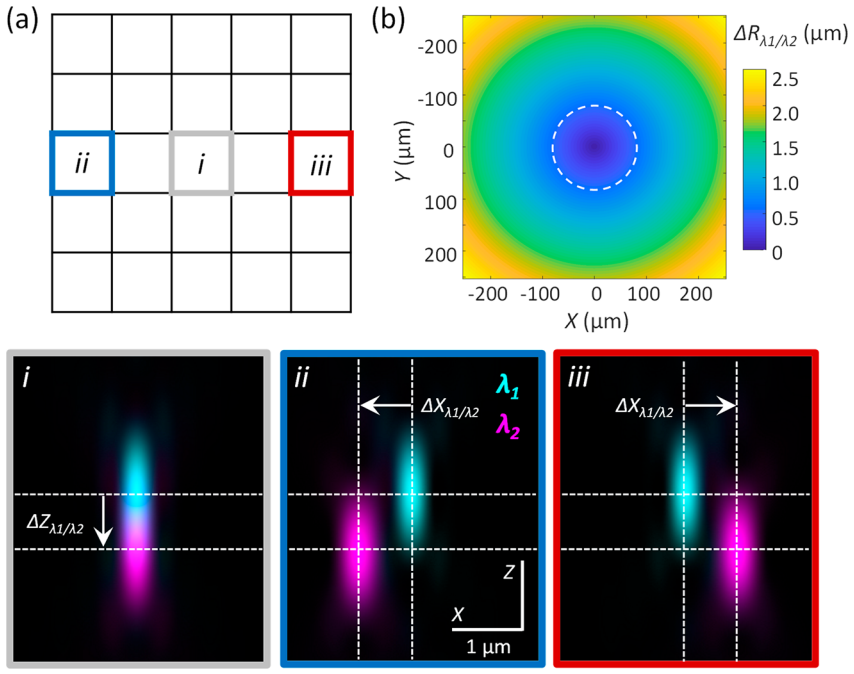

Figure 1. Chromatic aberration in dual-beam laser scanning microscopy. (a) Schematic representation of the imaging field of view. Due to axial chromatic aberration, at the center of the field of view (i) the two simulated focused beams centered at wavelengths λ_1 and λ_2 are shifted axially by $\Delta Z_{\lambda_1/\lambda_2}$. Due to axial and lateral chromatic aberration, at the edge of the field of view (ii) and (iii) the two simulated focused beams are shifted axially by $\Delta Z_{\lambda_1/\lambda_2}$ and laterally by $\Delta X_{\lambda_1/\lambda_2}$. (b) Measured lateral chromatic shifts $\Delta R_{\lambda_1/\lambda_2} = \sqrt{\Delta X_{\lambda_1/\lambda_2}^2 + \Delta Y_{\lambda_1/\lambda_2}^2}$ between the two focused beams across the imaging field of view. The lateral shifts increase linearly with the distance from the center of the field of view. White dashed lines correspond to lateral shifts of 0.80 μm. Microscope objective used: Zeiss W Plan-Apochromat 20×/1.0 DIC (Zeiss 20×).

in stimulated emission depletion (STED) microscopy,[21] with the advantage of facilitating coalignment of the beams. Nevertheless, these two methods do not correct for lateral chromatic aberration, which limits the effective size of the field of view in which the beams can be superimposed with a precision comparable to the lateral resolution. Alternatively, other studies have proposed mitigating lateral chromatic aberration by carefully designing the scanning system of the multiphoton microscope,[22] but ultimately the microscope objective has been shown to be the main source of chromatic aberration.[23] To solve this problem, the use of reflective microscope objectives has been proposed, but with limited spatial resolution and field of view[24,25] compared to what can be achieved with a single excitation wavelength and a standard low-magnification and high-numerical-aperture (high-NA) refractive objective. In addition, several postacquisition strategies have been developed to correct for chromatic aberration after signal detection, such as using sequential excitation at multiple wavelengths and a posteriori rescaling.[23] In all cases, this occurs at the expense of temporal resolution. We note that postacquisition methods are not applicable to all the multiphoton techniques using signals generated by two spatially overlapping beams, such as wavelength mixing,[16] coherent anti-Stokes Raman scattering (CARS),[26] and sum frequency generation (SFG).[27] Finally, chromatic aberration can be avoided by using a single wavelength to excite several chromophores.[28] However, this strategy requires some overlap of fluorophore absorption spectra, results in inefficient excitation of at least one of the fluorophores, and increases photobleaching of red-shifted fluorophores.[29] It also compromises the signal-to-noise ratio, as it is not possible to independently balance the different fluorescence signals. Therefore, until now, no method has been proposed to correct for both axial and lateral chromatic aberration without compromising field-of-view size, spatial and temporal resolution, or signal-to-noise ratio.

In contrast to previous work, here we propose a robust and light-efficient solution to correct for axial and lateral chromatic aberration in dual-beam multiphoton microscopy. Axial chromatic aberration is corrected by inserting a refractive phase mask designed to add pure defocus aberration between the two beams, while lateral chromatic aberration is canceled by actively changing the relative position of the two beams during raster scanning using a 2D steering mirror synchronized with the scanning system. We demonstrate the applicability of this strategy in the particular case of multicolor two-photon excitation by wavelength mixing, where two narrow-band laser beams centered at wavelengths λ_1 and λ_2 are temporally synchronized and spatially overlapped at the focal plane of a microscope objective, resulting in efficient two-photon (2P) and two-color, two-photon (2c−2P) excitation at wavelengths λ_1, λ_2, and $2/(\lambda_1^{-1} + \lambda_2^{-1})$. We demonstrate that this correction strategy enables three-color, two-photon imaging over an extended field of view with uncompromised spatial and temporal resolution and signal-to-noise ratio in live zebrafish embryos and fixed Brainbow mouse brain sections.

RESULTS AND DISCUSSION

We implemented our strategy on a dual-beam two-photon microscope optimized for mixed-wavelength excitation[30] (Figure 2a, Supporting Information (SI) section 1, Figure S1, and Tables S1 and S2). Two synchronous pulse trains generated by a titanium−sapphire oscillator centered at wavelength λ_1 = 850 nm and an optical parametric oscillator

https://doi.org/10.1021/acsphotonics.3c01104
ACS Photonics XXXX, XXX, XXX−XXX

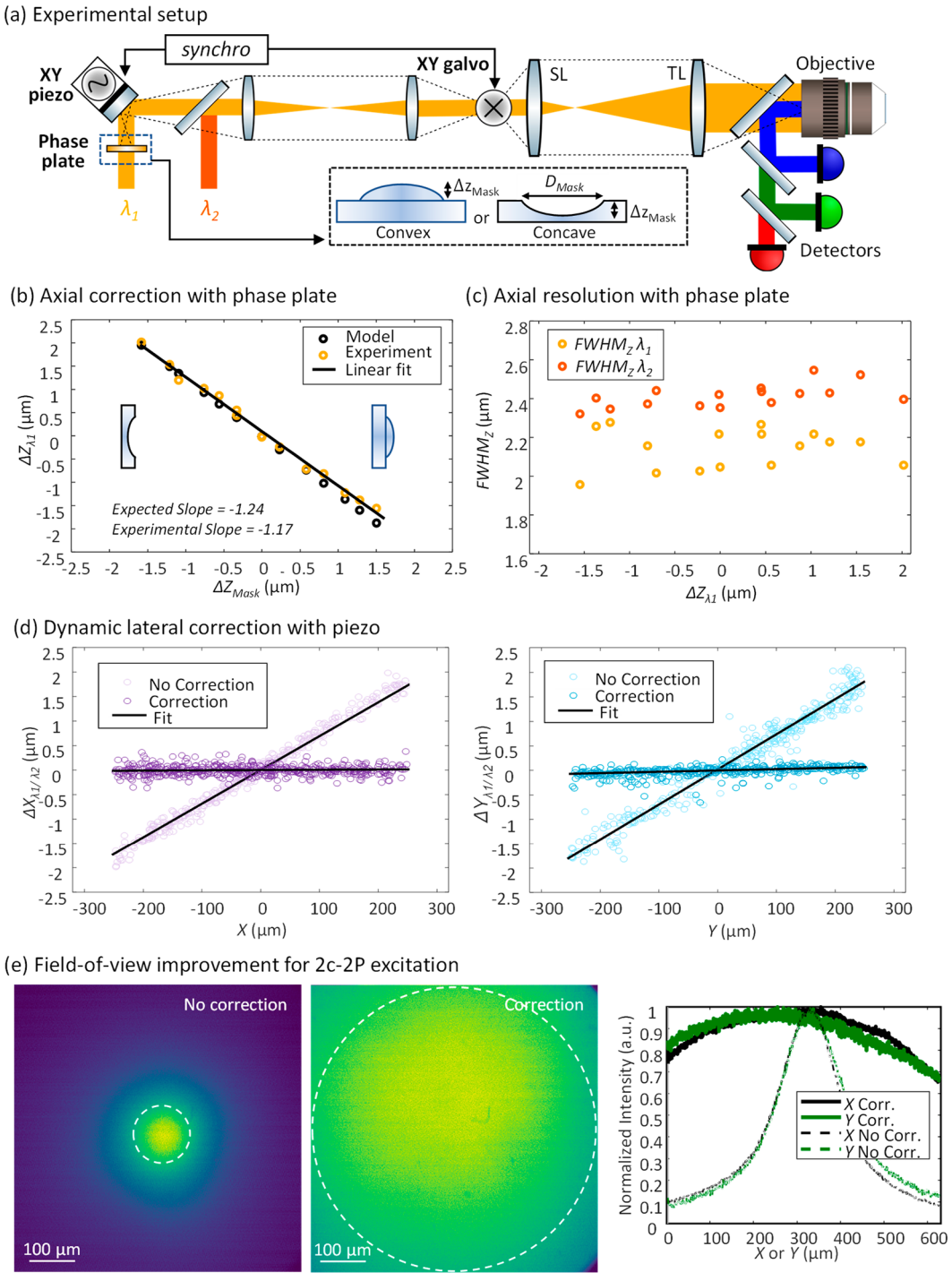

Figure 2. Chromatic aberration correction for dual-beam two-photon imaging. (a) Simplified optical setup of a two-photon point scanning microscope incorporating a pair of galvanometric mirrors optically conjugated with the back aperture of a microscope objective by a scan lens (SL) and tube lens (TL), a detection chain, and a module for dynamic chromatic aberration correction. The module consists of a phase mask, a piezo mirror, and two relay lenses. A complete schematic of the system is shown in Figure S1. (b, c) Axial chromatic correction with the refractive phase plate for two focused beams centered at wavelengths λ_1 = 850 nm and λ_2 = 1080 nm. By varying the amplitude (ΔZ_{Mask}) and the shape of the phase mask etching profile, the axial position of one of the two beams (ΔZ_{λ_1}) can be adjusted, while the axial resolution remains unchanged. (d) Dynamic correction of lateral chromatic aberration with the piezo mirror. The motion of the piezo mirror is synchronized with that of the linear galvanometer mirrors to compensate for the lateral chromatic shifts along the *X* and *Y* axes during the raster scanning of the two beams. (e) 2c−2P excitation efficiency across the imaging field of view with and without lateral chromatic correction. The field of view is 625 μm × 625 μm. White dashed lines indicate the areas where the fluorescence signal varies by less than 30%. Microscope objective used: Zeiss 20×.

centered at wavelength λ_2 = 1080 nm are spatially and temporally overlapped at the focal plane of the microscope equipped with two high-NA objectives (Olympus XLPLN25XWMP2 25×, NA = 1.05 and Zeiss W Plan-Apochromat 20×, NA = 1.0), known to have different chromatic properties.[23] Chromatic aberration introduced by

https://doi.org/10.1021/acsphotonics.3c01104
ACS Photonics XXXX, XXX, XXX−XXX

the scan lens, tube lens, and microscope objective are compensated by adding the appropriate amount of relative defocus and tip-tilt to one of the two laser beams before recombination (Figure 2a). To assess the effect of the correction on the point spread functions, we measured their axial extensions ($fwhm_Z$) and chromatic shifts along the X, Y, and Z axes ($\Delta X_{\lambda_1/\lambda_2}$, $\Delta Y_{\lambda_1/\lambda_2}$, and $\Delta Z_{\lambda_1/\lambda_2}$), as described in SI section 2. The axial chromatic shift between the beams is not expected to change considerably across the field of view. In a previous study,[23] we estimated it to vary by less than 1 μm over a 400 μm lateral field of view for several multiphoton objectives over the 850−1100 nm wavelength range. Therefore, it is corrected by introducing a lithographically etched static refractive phase mask (Carl Zeiss) designed to add pure defocus aberration (SI section 3 and Figure S2). The phase mask is first optically conjugated to a pair of linear galvanometer mirrors via a pair of identical focal lens relay lenses and then to the back aperture of the microscope objective via the scan and tube lenses (Figure 2a). A convex (respectively concave) refractive phase mask introduces a positive (respectively negative) amount of defocus at the objective back aperture, resulting in a positive (respectively negative) axial shift (ΔZ_{λ_1}) of the corrected beam focus after the objective (Figures 2b and S3a). The expected axial shift is proportional to the etch depth of the phase mask (ΔZ_{Mask}), with a proportionality factor given by eq 1 when the diameter of the mask is smaller than the diameter of the microscope objective back aperture (SI section 3):

$$\Delta Z = \frac{n_{SiO_2} - 1}{n\left(1 - \sqrt{1 - \left(\frac{D_{Mask} M_{Scan}}{D_{Pupil}}\right)^2 \frac{NA^2}{n^2}}\right)} \Delta Z_{Mask} \quad (1)$$

where n_{SiO_2} is the refractive index of SiO_2 at λ_1, n is the refractive index of the immersion medium at λ_1, D_{Pupil} is the back aperture diameter of the microscope objective, D_{Mask} is the diameter of the refractive phase mask, and M_{Scan} is the magnification of the scanning system composed of the scan lens and the tube lens.

To verify the prediction of the above model, we performed experiments with a series of masks with etch depths spanning ±2.0 in 0.25 μm increments, resulting in axial shifts of ±1.6 in 0.20 μm increments for the 25× Olympus objective and ±2.3 in 0.29 μm increments for the 20× Zeiss objective. The measured defocus is in very good agreement with our prediction, and importantly, the axial resolution is only slightly affected by the presence of the phase mask (Figures 2c and S3b and Table S3). The small deviations (<10%) between the predicted and measured defocus may be due to uncertainties in the values of the phase mask diameter, the magnification of the scanning system, or the etch depth. Small variations in axial resolution (<15%) (Figures 2c and S3b) are probably caused by imperfect conjugation between the phase mask and the back aperture of the microscope objective due to physical constraints on the optical path. Finally, after careful selection of the appropriate phase mask, the axial mismatch between the two focused beams was reduced to less than 0.10 μm for both microscope objectives with a marginal effect on axial resolution (Tables S2 and S3). We note that the achieved correction is better than the expected axial shift step between successive phase masks since the etching precision varies from one mask to another due to the manufacturing process.

Lateral chromatic aberration induces a wavelength-dependent radial shift that increases with the distance from the optical center (Figure 1). We proposed to correct this aberration with an active element, namely, a piezo-actuated steering mirror (S-331.2SH, Physik Instrumente, Germany),[31] installed on one of the beams and synchronized with the main scanning galvanometers (Figures 2a and S1). To determine the amplitude of the angular motion to be applied to the piezo mirror ($\Delta\alpha_{MaxX}$ and $\Delta\alpha_{MaxY}$), we derived a simple theoretical model linking the angular displacement to the relative chromatic shifts along the X and Y axes ($\Delta X/X_{\lambda_1/\lambda_2}$ and $\Delta Y/Y_{\lambda_1/\lambda_2}$) (SI section 4). We then estimated experimentally the relative chromatic shifts using second harmonic nanocrystals, as described in SI section 2. The shift between the 850 and 1080 nm foci reaches ±1.5 μm (respectively ±0.6 μm) at a location 200 μm from the center of the field of view when using the Zeiss 20× (respectively Olympus 25×) objective (Figures 2d and S3c), preventing efficient 2c−2P excitation (Figures 2e and S3d). The piezo mirror was then driven with the following amplitudes (see the derivation in SI section 4 and Table S4):

$$\Delta\alpha_{MaxX} = \pm\frac{1}{2} \arcsin\left(M_{Obj} \frac{\Delta X/X_{\lambda_1/\lambda_2} \times FOV_X}{FF \times 2f_{TubeObj}}\right) \times \frac{f_{Tube}}{f_{Scan}} \quad (2)$$

$$\Delta\alpha_{MaxY} = \pm\frac{1}{2} \arcsin\left(M_{Obj} \frac{\Delta Y/Y_{\lambda_1/\lambda_2} \times FOV_Y}{FF \times 2f_{TubeObj}}\right) \times \frac{f_{Tube}}{f_{Scan}} \quad (3)$$

where FOV_X and FOV_Y are the extensions of the field of view along the X and Y axes, respectively, $f_{TubeObj}$ is the nominal focal length of the tube lens of the objective, M_{Obj} is the magnification of the objective, FF is the image fill fraction, and f_{Scan} and f_{Tube} are the focal lengths of the scan and tube lenses, respectively.

After optimization, lateral chromatic shifts are reduced to less than 0.20 μm for both microscope objectives over their entire nominal fields of view (707 μm × 707 μm for the Zeiss 20× and 510 μm × 510 μm for the Olympus 25×), while the axial shifts remain unaffected (Figure S4). In turn, this adaptive correction is the key to efficient 2c−2P excitation over the entire field of view. In the case of the Zeiss 20×, which is particularly chromatic, our technique provides a 5-fold increase in the radius of the effective field of view (i.e., a 25-fold increase in surface area) for 2c−2P excitation in a homogeneous fluorescent sample (Figures 2e and S3d). After correction, the 2c−2P excitation profile decreases by less than 30% at the edge of the field of view for both objectives. This residual loss is mainly due to the vignetting of the excitation beams in the scanning path and the fluorescence signal in the detection path (Figure S5). We confirmed the efficiency of our approach for bioimaging by acquiring 2c−2P images of a green fluorescent protein (GFP)-labeled live zebrafish embryo and fixed yellow fluorescent protein (YFP)-labeled mouse brain (Figure S6) and obtained the same benefit: while the 2c−2P signal drops by about 30% 60 μm away from the center of the field of view in the absence of correction, it is efficiently obtained over the entire field of view with the adaptive correction.

https://doi.org/10.1021/acsphotonics.3c01104
ACS Photonics XXXX, XXX, XXX−XXX

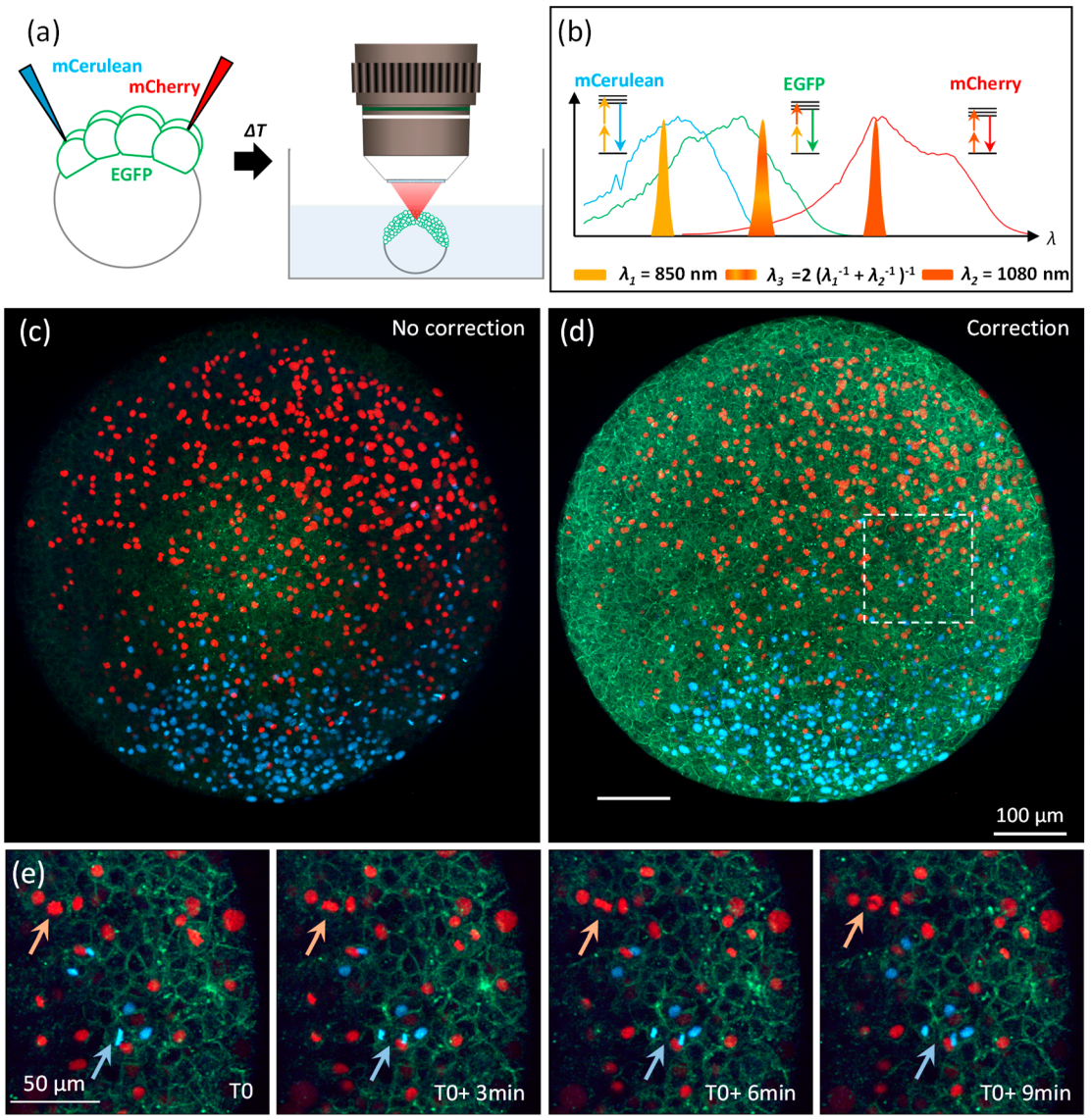

Figure 3. Multicolor two-photon imaging of a live zebrafish embryo with dynamic chromatic correction. (a) Zebrafish embryos labeled with mCerulean, EGFP, and mCherry are mounted in an imaging chamber filled with 0.20% agarose and embryo medium for imaging. (b) Two-photon excitation spectra of the corresponding three fluorescent proteins and two-photon excitation wavelengths used for imaging (λ_1 = 850 nm, λ_2 = 1080 nm, and λ_3 = 950 nm). (c, d) Maximal intensity projections computed from a 3D *z*-stack acquired over a field of view of 740 μm × 740 μm and a depth of 200 μm (c) without and (d) with lateral chromatic correction. (e) Series of ROIs extracted from 4D *z*-stacks acquired over the same volume with a time delay of 3 min. Red and blue arrows indicate cells undergoing division. Microscope objective used: Zeiss 20×.

Our approach can be directly extended to achieve chromatically corrected color multiphoton imaging over large fields of view. As recalled earlier, mixing two narrow-band pulses allows simultaneous two-photon excitation of multiple spectrally distinct fluorophores through degenerate (one-color) and nondegenerate (two-color) processes. Our chromatic correction implementation does not compromise acquisition speed and operates seamlessly with bidirectional line scanning rates of at least 400 Hz. As a first application of our approach, we acquired trichromatic 3D+T images of developing zebrafish embryos labeled with three different fluorescent proteins. Embryos at 5 hpf expressed mCerulean and mCherry in the nuclei of two cell subpopulations and GFP in all cell membranes (Figure 3a,b and SI section 6). Simultaneous imaging of the distribution of the three fluorescent proteins over the entire diameter of the embryo is possible only with chromatic aberration correction (Figure 3c,d and Supplementary Video S1). In turn, the presence of the wavelength mixing signal confirms that the three channels are registered with submicrometer precision over the entire field of view. The acquisition of 3D *z*-stacks with a time step of 3 or 4 min allows us to track the cells and to detect divisions in the two color-tagged subpopulations while imaging cell shapes with the GFP signal (Figure 3e and Supplementary Video S2).

Tile-based mapping over large areas of multicolor-labeled tissue is another application that can directly benefit from the extended field of view and signal homogeneity provided by our approach. Figures 4 and S7 show such tiled acquisitions in brain sections of a Brainbow transgenic mouse expressing the three fluorescent proteins mTurquoise2, mEYFP, and tdTomato in neural cells in a stochastic and mutually exclusive manner (SI section 7). Adaptive chromatic correction restores signal homogeneity across the entire field of view of the objective, which removes illumination artifacts during mosaic

https://doi.org/10.1021/acsphotonics.3c01104
ACS Photonics XXXX, XXX, XXX−XXX

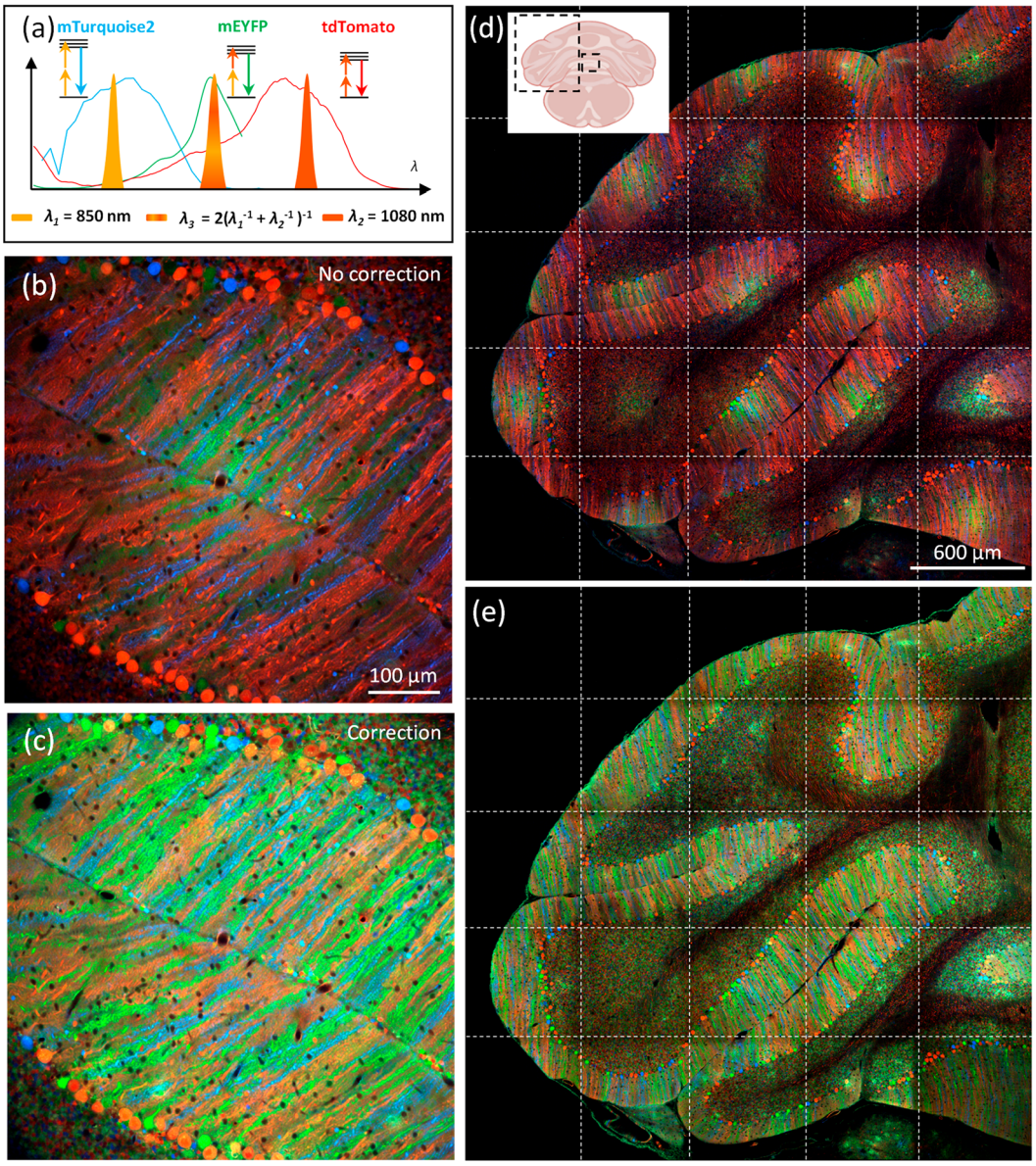

Figure 4. Multicolor two-photon mosaic imaging in the cerebellum of a Brainbow transgenic mouse with dynamic chromatic correction. (a) Two-photon absorption spectra of the fluorescent proteins expressed by the Brainbow transgene (mTurquoise2, mEYFP, and tdTomato) and two-photon excitation wavelengths used for imaging (λ_1 = 850 nm, λ_2 = 1080 nm, and λ_3 = 950 nm). (b, c) Individual tiles acquired on an area of 625 μm × 625 μm (b) without and (c) with lateral chromatic correction. (d, e) 5 × 5 mosaics of tiles acquired from a mouse brain cerebellum slice (d) without and (e) with lateral chromatic correction, corresponding to a scanned area of 2925 μm × 2950 μm. White dashed lines indicate tile borders. Microscope objective used: Zeiss 20×.

acquisitions and results in an overall gain in signal-to-noise ratio. It also enables relaxation of the constraints on the choice of the microscope objective and thus the selection of the most appropriate objective for the application. Currently, the range of commercially available microscope objectives compatible with multiphoton microscopy that present a large field of view and high numerical aperture is very limited. These objectives exhibit either pronounced field curvature (Figure S4) or a pronounced amount of chromatic aberration.[23] Consequently, our approach should allow us to reduce acquisition times and facilitate data reconstruction for mosaic acquisitions. For example, when using 625 μm × 625 μm fields of view (Figure 4), the number of images required to cover a given area can be divided by about 4 compared to a reference study using 300 μm × 360 μm fields of view,[30] with the added benefit of removing field curvature. These advantages should be particularly useful in the context of slide scanners and serial tomography,[30] where thousands of fields of view are acquired and stitched together.

CONCLUSION

Chromatic aberration is present in most microscope objectives and scanning systems and has been an unsolved problem in the development of broadband multiphoton imaging. In this work, we demonstrate an effective and generic approach for adaptive chromatic correction in dual-beam multiphoton microscopy. We believe that this method should directly benefit all situations in which two focused beams centered at different wavelengths are used in multiphoton microscopy, as for example in the following cases: two-photon or three-photon

https://doi.org/10.1021/acsphotonics.3c01104
ACS Photonics XXXX, XXX, XXX−XXX

imaging at two colors, combined two-photon and three-photon imaging, photomanipulation and imaging at different wavelengths, and multicolor two-photon imaging by wavelength mixing. Although demonstrated in the case of two beams, the approach described here could be generalized to more than two beams. However, it is particularly interesting in the case of excitation by wavelength mixing, since by correction of only two excitation wavelengths, all excitation processes resulting from wavelength mixing are intrinsically corrected. Importantly, the strategy described here does not compromise field-of-view size, spatial and temporal resolution, and excitation and detection efficiency. It is also straightforward to use and implement, as it is directly compatible with a standard multiphoton microscope, requires the introduction of only four optical elements in the scanning path (resulting in a light efficiency on the order of 85%), and operates seamlessly during data recording after a single calibration procedure. More generally, the work described here should be of interest for other dual-beam microscopy techniques that are based on the spatial overlap between two focused beams, such as STED,[32] CARS, pump−probe,[33] or SFG techniques.

■ ASSOCIATED CONTENT

Supporting Information

The Supporting Information is available free of charge at https://pubs.acs.org/doi/10.1021/acsphotonics.3c01104.

Detailed optical setup; recording and analysis of point spread functions from SHG nanoprobes; pure defocus with refractive phase masks to correct axial chromatic aberration; piezo mirror to correct lateral chromatic aberration; 2c−2P fluorescence signal across the scanned field of view with lateral chromatic correction; sample preparation and imaging conditions for zebrafish embryos; sample preparation and imaging conditions for fixed Brainbow mouse brain slices; chromatically corrected 2D mosaic acquisition of a Brainbow mouse brain slice for the Olympus XLPLN25XWMP2 microscope objective (PDF)

Supplementary Video 1 (MP4)

Supplementary Video 2 (MP4)

■ AUTHOR INFORMATION

Corresponding Authors

Pierre Mahou − *Laboratoire d'Optique et Biosciences, Ecole Polytechnique, CNRS, INSERM, Institut Polytechnique de Paris, 91128 Palaiseau, France;* orcid.org/0000-0003-4452-1011; Email: pierre.mahou@polytechnique.edu

Emmanuel Beaurepaire − *Laboratoire d'Optique et Biosciences, Ecole Polytechnique, CNRS, INSERM, Institut Polytechnique de Paris, 91128 Palaiseau, France;* orcid.org/0000-0002-2082-8214; Email: emmanuel.beaurepaire@polytechnique.edu

Authors

Hugo Blanc − *Laboratoire d'Optique et Biosciences, Ecole Polytechnique, CNRS, INSERM, Institut Polytechnique de Paris, 91128 Palaiseau, France*

Gabriel Kaddour − *Sorbonne Université, INSERM, CNRS, Institut de la Vision, 75012 Paris, France;* orcid.org/0009-0008-5392-4713

Nicolas B. David − *Laboratoire d'Optique et Biosciences, Ecole Polytechnique, CNRS, INSERM, Institut Polytechnique de Paris, 91128 Palaiseau, France*

Willy Supatto − *Laboratoire d'Optique et Biosciences, Ecole Polytechnique, CNRS, INSERM, Institut Polytechnique de Paris, 91128 Palaiseau, France;* orcid.org/0000-0002-4562-9166

Jean Livet − *Sorbonne Université, INSERM, CNRS, Institut de la Vision, 75012 Paris, France;* orcid.org/0000-0003-3079-4908

Complete contact information is available at: https://pubs.acs.org/10.1021/acsphotonics.3c01104

Author Contributions

H.B., W.S., E.B., and P.M. designed the study. N.B.D., E.B., and W.S. designed the zebrafish demonstration experiments. H.B., G.K., and P.M. designed the mouse demonstration experiments. G.K. and J.L. prepared and provided the Brainbow mouse samples. N.B.D. prepared and provided the zebrafish samples. H.B. and P.M. performed the experiments and analyzed the data. H.B., W.S., E.B., and P.M. wrote the manuscript with inputs from all other authors.

Notes

The authors declare no competing financial interest.

■ ACKNOWLEDGMENTS

We thank all members of the Laboratory for Optics and Biosciences for discussions on biomicroscopy, Jean-Marc Sintes for mechanical help, Emilie Menant and Isabelle Lamarre-Jouenne for fish care. We thank the animal housing facility at Institut de la Vision. We thank Mitchell Sandoe (MBF) for assistance with control software. This work was supported by the European Research Council (Horizon 2020 Program, Grant 951330 HOPE), the Agence Nationale de la Recherche (ANR-EQPX-0029, ANR-10-INBS-04, ANR-19-CE16-0019, ANR-18-IAHU-01, and ANR-20-CE13-0016-03), and Région Ile de France (DIM Elicit).

■ REFERENCES

(1) Wang, M.; Da, Y.; Tian, Y. Fluorescent Proteins and Genetically Encoded Biosensors. *Chem. Soc. Rev.* **2023**, *52* (4), 1189−1214.

(2) Dumas, L.; Clavreul, S.; Michon, F.; Loulier, K. Multicolor Strategies for Investigating Clonal Expansion and Tissue Plasticity. *Cell. Mol. Life Sci.* **2022**, *79* (3), 141.

(3) Denk, W.; Strickler, J. H.; Webb, W. W. Two-Photon Laser Scanning Fluorescence Microscopy. *Science* **1990**, *248* (4951), 73−76.

(4) Helmchen, F.; Denk, W. Deep Tissue Two-Photon Microscopy. *Nat. Methods* **2005**, *2* (12), 932−940.

(5) Grienberger, C.; Giovannucci, A.; Zeiger, W.; Portera-Cailliau, C. Two-Photon Calcium Imaging of Neuronal Activity. *Nat. Rev. Methods Primers* **2022**, *2* (1), 66.

(6) Ramirez, D. M. O.; Ajay, A. D.; Goldberg, M. P.; Meeks, J. P. Serial Multiphoton Tomography and Analysis of Vol.tric Images of the Mouse Brain. *Neuromethods* **2019**, *148*, 195−224.

(7) Ueki, H.; Wang, I. H.; Zhao, D.; Gunzer, M.; Kawaoka, Y. Multicolor Two-Photon Imaging of in Vivo Cellular Pathophysiology upon Influenza Virus Infection Using the Two-Photon IMPRESS. *Nat. Protoc.* **2020**, *15* (3), 1041−1065.

(8) Boutillon, A.; Escot, S.; Elouin, A.; Jahn, D.; González-Tirado, S.; Starruß, J.; Brusch, L.; David, N. B. Guidance by Followers Ensures Long-Range Coordination of Cell Migration through α-Catenin Mechanoperception. *Dev. Cell* **2022**, *57* (12), 1529−1544.

(9) Lecoq, J.; Orlova, N.; Grewe, B. F. Wide. Fast. Deep: Recent Advances in Multiphoton Microscopy of in Vivo Neuronal Activity. *J. Neurosci.* **2019**, *39* (46), 9042−9052.
(10) Gigan, S.; Katz, O.; De Aguiar, H. B.; Andresen, E. R.; Aubry, A.; Bertolotti, J.; Bossy, E.; Bouchet, D.; Brake, J.; Brasselet, S.; Bromberg, Y.; Cao, H.; Chaigne, T.; Cheng, Z.; Choi, W.; Čižmár, T.; Cui, M.; Curtis, V. R.; Defienne, H.; Hofer, M.; Horisaki, R.; Horstmeyer, R.; Ji, N.; LaViolette, A. K.; Mertz, J.; Moser, C.; Mosk, A. P.; Pégard, N. C.; Piestun, R.; Popoff, S.; Phillips, D. B.; Psaltis, D.; Rahmani, B.; Rigneault, H.; Rotter, S.; Tian, L.; Vellekoop, I. M.; Waller, L.; Wang, L.; Weber, T.; Xiao, S.; Xu, C.; Yamilov, A.; Yang, C.; Yılmaz, H. Roadmap on Wavefront Shaping and Deep Imaging in Complex Media. *J. Phys.: Photonics* **2022**, *4* (4), 042501.
(11) Seo, J.; Sim, Y.; Kim, J.; Kim, H.; Cho, I.; Nam, H.; Yoon, Y. G.; Chang, J. B. PICASSO Allows Ultra-Multiplexed Fluorescence Imaging of Spatially Overlapping Proteins without Reference Spectra Measurements. *Nat. Commun.* **2022**, *13* (1), 2475.
(12) Bares, A. J.; Mejooli, M. A.; Pender, M. A.; Leddon, S. A.; Tilley, S.; Lin, K.; Dong, J.; Kim, M.; Fowell, D. J.; Nishimura, N.; Schaffer, C. B. Hyperspectral Multiphoton Microscopy for in Vivo Visualization of Multiple, Spectrally Overlapped Fluorescent Labels. *Optica* **2020**, *7* (11), 1587.
(13) Ogilvie, J. P.; Débarre, D.; Solinas, X.; Martin, J.-L.; Beaurepaire, E.; Joffre, M. Use of Coherent Control for Selective Two-Photon Fluorescence Microscopy in Live Organisms. *Opt. Express* **2006**, *14* (2), 759.
(14) Isobe, K.; Suda, A.; Tanaka, M.; Kannari, F.; Kawano, H.; Mizuno, H.; Miyawaki, A.; Midorikawa, K. Multifarious Control of Two-Photon Excitation of Multiple Fluorophores Achieved by Phase Modulation of Ultra-Broadband Laser Pulses. *Opt. Express* **2009**, *17* (16), 13737.
(15) Chou, L.-T.; Wu, S.-H.; Hung, H.-H.; Lin, W.-Z.; Chen, Z.-P.; Ivanov, A. A.; Chia, S.-H. Compact Multicolor Two-Photon Fluorescence Microscopy Enabled by Tailorable Continuum Generation from Self-Phase Modulation and Dispersive Wave Generation. *Opt. Express* **2022**, *30* (22), 40315.
(16) Mahou, P.; Zimmerley, M.; Loulier, K.; Matho, K. S.; Labroille, G.; Morin, X.; Supatto, W.; Livet, J.; Débarre, D.; Beaurepaire, E. Multicolor Two-Photon Tissue Imaging by Wavelength Mixing. *Nat. Methods* **2012**, *9* (8), 815−818.
(17) Rakhymzhan, A.; Leben, R.; Zimmermann, H.; Günther, R.; Mex, P.; Reismann, D.; Ulbricht, C.; Acs, A.; Brandt, A. U.; Lindquist, R. L.; Winkler, T. H.; Hauser, A. E.; Niesner, R. A. Synergistic Strategy for Multicolor Two-Photon Microscopy: Application to the Analysis of Germinal Center Reactions in Vivo. *Sci. Rep.* **2017**, *7* (1), 7101.
(18) Keller, H. E. Objective Lenses for Confocal Microscopy. In *Handbook of Biological Confocal Microscopy*, 3rd ed.; Springer, 2006; pp 145−161. DOI: 10.1007/978-0-387-45524-2_7.
(19) Andresen, V.; Alexander, S.; Heupel, W.; Hirschberg, M.; Hoffman, R. M.; Friedl, P. Infrared Multiphoton Microscopy: Subcellular-Resolved Deep Tissue Imaging. *Curr. Opin. Biotechnol.* **2009**, *20* (1), 54−62.
(20) Botcherby, E. J.; Juskaitis, R.; Booth, M. J.; Wilson, T. Aberration-Free Optical Refocusing in High Numerical Aperture Microscopy. *Opt. Lett.* **2007**, *32* (14), 2007−2009.
(21) Mahou, P.; Curry, N.; Pinotsi, D.; Kaminski Schierle, G.; Kaminski, C. Stimulated Emission Depletion Microscopy to Study Amyloid Fibril Formation. *Proc. SPIE* **2015**, *9331*, 93310U.
(22) Negrean, A.; Mansvelder, H. D. Optimal Lens Design and Use in Laser-Scanning Microscopy. *Biomed. Opt. Express* **2014**, *5* (5), 1588−1609.
(23) Mahou, P.; Malkinson, G.; Chaudan, É.; Gacoin, T.; Beaurepaire, E.; Supatto, W. Metrology of Multiphoton Microscopes Using Second Harmonic Generation Nanoprobes. *Small* **2017**, *13* (42), 1701442.
(24) Amirsolaimani, B.; Cromey, B.; Peyghambarian, N.; Kieu, K. All-Reflective Multiphoton Microscope. *Opt. Express* **2017**, *25* (19), 23399.
(25) Akhoundi, F.; Peyghambarian, N. Single-Cavity Dual-Wavelength All-Fiber Femtosecond Laser for Multimodal Multiphoton Microscopy. *Biomed. Opt. Express* **2020**, *11* (5), 2761.
(26) Cheng, J. X.; Jia, Y. K.; Zheng, G.; Xie, X. S. Laser-Scanning Coherent Anti-Stokes Raman Scattering Microscopy and Applications to Cell Biology. *Biophys. J.* **2002**, *83* (1), 502−509.
(27) Hanninen, A.; Shu, M. W.; Potma, E. O. Hyperspectral Imaging with Laser-Scanning Sum-Frequency Generation Microscopy. *Biomed. Opt. Express* **2017**, *8* (9), 4230.
(28) Tillo, S. E.; Hughes, T. E.; Makarov, N. S.; Rebane, A.; Drobizhev, M. A New Approach to Dual-Color Two-Photon Microscopy with Fluorescent Proteins. *BMC Biotechnol.* **2010**, *10*, 6.
(29) Mahou, P.; Vermot, J.; Beaurepaire, E.; Supatto, W. Multicolor Two-Photon Light-Sheet Microscopy. *Nat. Methods* **2014**, *11* (6), 600−601.
(30) Abdeladim, L.; Matho, K. S.; Clavreul, S.; Mahou, P.; Sintes, J. M.; Solinas, X.; Arganda-Carreras, I.; Turney, S. G.; Lichtman, J. W.; Chessel, A.; Bemelmans, A. P.; Loulier, K.; Supatto, W.; Livet, J.; Beaurepaire, E. Multicolor Multiscale Brain Imaging with Chromatic Multiphoton Serial Microscopy. *Nat. Commun.* **2019**, *10* (1), 1662.
(31) Tapos, F. M.; Edinger, D. J.; Hilby, T. R.; Ni, M. S.; Holmes, B. C.; Stubbs, D. M. High Bandwidth Fast Steering Mirror. *Proc. SPIE* **2005**, *5877*, 587707.
(32) ter Veer, M. J. T.; Pfeiffer, T.; Nägerl, U. V. Two-Photon STED Microscopy for Nanoscale Imaging of Neural Morphology in Vivo. *Methods Mol. Biol.* **2017**, *1663*, 45−64.
(33) Fischer, M. C.; Wilson, J. W.; Robles, F. E.; Warren, W. S. Invited Review Article: Pump-Probe Microscopy. *Rev. Sci. Instrum.* **2016**, *87* (3), 031101.

https://doi.org/10.1021/acsphotonics.3c01104
ACS Photonics XXXX, XXX, XXX−XXX